Chapter 1

Nuclear Reaction Kinematics and Spectroscopy

> *"The energy of the outgoing particle is a spectrometer for the excitation of the residual nucleus, once Q-value kinematics are under control."*
>
> reaction spectroscopy [6, 1]

The preceding lecture classified reaction mechanisms. This chapter connects measured kinetic energies and angles to nuclear excitation energies: two-body momentum and energy conservation, the Q-value, the full non-relativistic relation among K_a, K_b, θ, and masses, thresholds for endothermic reactions, neutron capture on ^{238}U as a worked example, and the idea of resonant energy dependence of the cross section [6, 1, 14, 2].

1.1 Experimental geometry and what is measured

Consider the binary reaction

$$X(a,b)Y \qquad \text{or} \qquad a + X \to b + Y \tag{1.1}$$

in the laboratory frame with target X at rest. Projectile a has kinetic energy K_a and momentum $\mathbf{p}_a$. Product b is detected at laboratory angle θ with kinetic energy K_b and momentum $\mathbf{p}_b$. Residual Y recoils at angle ϕ with kinetic energy K_Y and momentum $\mathbf{p}_Y$.

Measurable quantities are typically K_a (set by the accelerator), θ, and K_b (from the detector). The residual kinetic energy K_Y is usually not measured directly. Nuclear data tables supply rest masses. The unknown of spectroscopic interest is often the excitation energy ΔE of Y [6, 1].

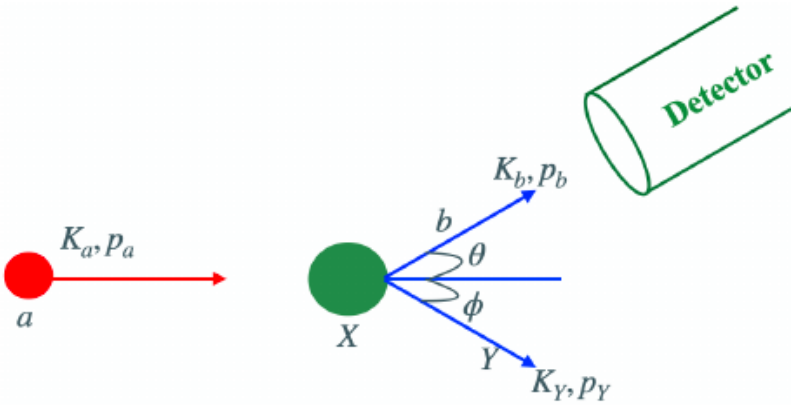

Figure 1.1: Laboratory setup for a two-body reaction $X(a,b)Y$: projectile a, target X, light product b at angle θ, residual Y at angle ϕ, and a detector that measures K_b (lecture figure).

1.2 Conservation laws

1.2.1 Momentum

With the beam along $+x$ and the reaction in the xy plane,

$$p_a = p_b \cos\theta + p_Y \cos\phi, \tag{1.2}$$

$$0 = p_b \sin\theta - p_Y \sin\phi. \tag{1.3}$$

(The target is at rest, so initial $p_y = 0$.)

1.2.2 Energy and Q-value

Including rest energies and allowing residual excitation ΔE,

$$m_a c^2 + m_X c^2 + K_a = m_b c^2 + m_Y c^2 + K_b + K_Y + \Delta E. \tag{1.4}$$

Define the reaction **Q-value** from ground-state rest masses,

$$Q \equiv (m_a + m_X - m_b - m_Y)c^2. \tag{1.5}$$

Then (1.4) becomes

$$Q + K_a = K_b + K_Y + \Delta E. \tag{1.6}$$

- $Q > 0$: **exoergic** (exothermic); energy is released.
- $Q < 0$: **endoergic** (endothermic); a minimum beam energy is required (Section 1.9.2).

If Y is left in its ground state, set $\Delta E = 0$. Excited states appear as discrete peaks at lower K_b for fixed θ [6, 1, 14].

1.2.3 Invariant definition and exact CM energy

The mass-difference definition of Q is frame independent. Introduce the Mandelstam invariant s, with units of energy squared,

$$s = (E_a + E_X)^2 - c^2|\mathbf{p}_a + \mathbf{p}_X|^2. \tag{1.7}$$

For a target at rest, $E_X = m_X c^2$ and

$$s = (m_a c^2)^2 + (m_X c^2)^2 + 2m_X c^2(m_a c^2 + K_a). \tag{1.8}$$

Thus the exact energy available in the CM is $\sqrt{s}$. If the residual is excited, its effective rest mass is

$$m_Y^* = m_Y + \frac{\Delta E}{c^2}, \qquad Q^* = Q - \Delta E. \tag{1.9}$$

The final CM momentum follows without choosing a laboratory angle:

$$p_f^* c = \frac{\sqrt{\lambda(s, (m_b c^2)^2, (m_Y^* c^2)^2)}}{2\sqrt{s}}, \qquad \lambda(x, y, z) = x^2 + y^2 + z^2 - 2xy - 2xz - 2yz. \tag{1.10}$$

The channel is open only when the square root is real. Equations (1.8)–(1.10) are the exact relativistic two-body result; the following laboratory formula is their low-energy reduction [6, 14].

Physical meaning of ΔE. Each bound level of Y produces a kinematic locus $K_b(\theta)$. Measuring K_b at known θ and K_a is nuclear level spectroscopy via reaction kinematics.

1.3 Eliminating the unobserved residual

Nuclear kinetic energies of a few MeV on mass $\sim A \times 931\,\text{MeV}$ justify the non-relativistic relations

$$K_Y = \frac{p_Y^2}{2m_Y}, \qquad p_a^2 = 2m_a K_a, \qquad p_b^2 = 2m_b K_b. \tag{1.11}$$

From (1.2)–(1.3),

$$p_Y \cos\phi = p_a - p_b \cos\theta, \qquad p_Y \sin\phi = p_b \sin\theta. \tag{1.12}$$

Squaring and adding eliminates ϕ:

$$p_Y^2 = (p_a - p_b\cos\theta)^2 + (p_b \sin\theta)^2 = p_a^2 + p_b^2 - 2p_a p_b \cos\theta. \tag{1.13}$$

Therefore

$$K_Y = \frac{p_Y^2}{2m_Y} = \frac{m_a}{m_Y}K_a + \frac{m_b}{m_Y}K_b - \frac{2}{m_Y}\sqrt{m_a m_b K_a K_b}\,\cos\theta. \tag{1.14}$$

Substitute (1.14) into (1.6):

$$Q + K_a = K_b + \frac{m_a}{m_Y}K_a + \frac{m_b}{m_Y}K_b - \frac{2}{m_Y}\sqrt{m_a m_b K_a K_b}\,\cos\theta + \Delta E. \tag{1.15}$$

Collecting terms,

$$Q + K_a\Big(1 - \frac{m_a}{m_Y}\Big) = K_b\Big(1 + \frac{m_b}{m_Y}\Big) - \frac{2}{m_Y}\sqrt{m_a m_b K_a K_b}\,\cos\theta + \Delta E. \tag{1.16}$$

Solving for the excitation energy,

$$\Delta E = Q - K_b\Big(1 + \frac{m_b}{m_Y}\Big) + K_a\Big(1 - \frac{m_a}{m_Y}\Big) + \frac{2}{m_Y}\sqrt{m_a m_b K_a K_b}\,\cos\theta. \tag{1.17}$$

All quantities on the right are either tabulated (Q, masses) or measured (K_a, K_b, θ). Equation (1.17) is the working formula of two-body reaction spectroscopy in the non-relativistic limit [6, 1].

1.3.1 From CM observables to laboratory observables

For a non-relativistic binary exit channel, let V be the CM speed in the laboratory and u_b the speed of b in the CM. Galilean velocity addition gives

$$\mathbf{v}_{b,\mathrm{lab}} = V\hat{\mathbf{x}} + u_b(\cos\theta_{\mathrm{cm}}\hat{\mathbf{x}} + \sin\theta_{\mathrm{cm}}\hat{\mathbf{y}}). \tag{1.18}$$

Therefore, with $\gamma_k \equiv V/u_b$,

$$\tan\theta_{\mathrm{lab}} = \frac{\sin\theta_{\mathrm{cm}}}{\gamma_k + \cos\theta_{\mathrm{cm}}}, \tag{1.19}$$

$$K_{b,\mathrm{lab}} = \frac{1}{2}m_b\left(V^2 + u_b^2 + 2Vu_b\cos\theta_{\mathrm{cm}}\right). \tag{1.20}$$

Solid angles also transform. Away from kinematic turning points, $\mathrm{d}\Omega = 2\pi\,\mathrm{d}(\cos\theta)$. Write

$$\cos\theta_{\mathrm{lab}} = \frac{\gamma_k + \cos\theta_{\mathrm{cm}}}{\sqrt{1 + 2\gamma_k\cos\theta_{\mathrm{cm}} + \gamma_k^2}}$$

and differentiate with respect to $\mu \equiv \cos\theta_{\mathrm{cm}}$. With $N = \gamma_k + \mu$ and $D = \sqrt{1 + 2\gamma_k\mu + \gamma_k^2}$,

$$\frac{\mathrm{d}(\cos\theta_{\mathrm{lab}})}{\mathrm{d}\mu} = \frac{D - N\cdot(\gamma_k/D)}{D^2} = \frac{D^2 - N\gamma_k}{D^3} = \frac{1 + \gamma_k\mu}{D^3}, \tag{1.21}$$

so

$$\left|\frac{\mathrm{d}\Omega_{\mathrm{lab}}}{\mathrm{d}\Omega_{\mathrm{cm}}}\right| = \frac{|1 + \gamma_k\cos\theta_{\mathrm{cm}}|}{(1 + 2\gamma_k\cos\theta_{\mathrm{cm}} + \gamma_k^2)^{3/2}}, \quad \left(\frac{\mathrm{d}\sigma}{\mathrm{d}\Omega}\right)_{\mathrm{lab}} = \left(\frac{\mathrm{d}\sigma}{\mathrm{d}\Omega}\right)_{\mathrm{cm}}\left|\frac{\mathrm{d}\Omega_{\mathrm{cm}}}{\mathrm{d}\Omega_{\mathrm{lab}}}\right|. \tag{1.22}$$

One CM angle can map to a sharply focused laboratory cone; in some endothermic reactions two kinematic branches can occur at one forward laboratory angle. This is why an angular distribution must name its frame [6, 1].

Caution

Masses in (1.17) must be consistent (nuclear or atomic with the same convention on both sides of Q). Evaluated atomic masses from AME2020 are appropriate when electron numbers cancel. For precise work one uses relativistic kinematics; the structure of the argument is

unchanged [6, 14, 27].

1.4 Quadratic equation for K_b and kinematic loci

For fixed K_a, θ, and ΔE, equation (1.15) is quadratic in $\sqrt{K_b}$ (or in K_b after clearing the square root). Writing $x = \sqrt{K_b}$,

$$\Big(1 + \frac{m_b}{m_Y}\Big)x^2 - \frac{2\cos\theta}{m_Y}\sqrt{m_a m_b K_a}\; x + \Big[K_a\Big(\frac{m_a}{m_Y} - 1\Big) - Q + \Delta E\Big] = 0. \tag{1.23}$$

A physical root needs $K_b > 0$ and a non-negative discriminant. This restricts the allowed beam energy, angle, and excitation, and underlies the threshold formulae [6, 1].

1.5 Threshold for endothermic reactions

At threshold the products have no relative momentum in the CM; in the laboratory they move together, because setting both final laboratory momenta to zero would violate momentum conservation. With $M_f^* = m_b + m_Y + \Delta E/c^2$, the invariant condition is $s_{\rm th} = (M_f^* c^2)^2$. Combining it with (1.8) gives the **exact** laboratory threshold

$$K_a^{\rm th} = \frac{(M_f^*)^2 - (m_a + m_X)^2}{2m_X}\, c^2. \tag{1.24}$$

Since $Q^* = Q - \Delta E = (m_a + m_X - M_f^*)c^2$, equivalently

$$K_a^{\rm th} = -Q^*\left(1 + \frac{m_a}{m_X}\right) + \frac{(Q^*)^2}{2m_X c^2}. \tag{1.25}$$

The final term is the small relativistic mass correction. Dropping it gives the standard non-relativistic result

$$K_a^{\rm th} = (-Q + \Delta E)\frac{m_a + m_X}{m_X} = (-Q + \Delta E)\Big(1 + \frac{m_a}{m_X}\Big). \tag{1.26}$$

The factor $(1 + m_a/m_X) > 1$ appears because part of the beam energy is tied up in CM motion. For $Q^* < 0$ the threshold is positive. Even if the ground-state reaction is exoergic, a level with $\Delta E > Q$ has $Q^* < 0$ and therefore a threshold [6, 1, 14].

Exoergic case. If $Q^* > 0$, the channel has zero mass-difference threshold (neglecting angular-momentum constraints). Charged-particle cross sections can still be strongly suppressed at low energy; tunnelling makes the Coulomb barrier a suppression, not a sharp kinematic threshold. At $Q^* = 0$ the channel opens at zero energy with vanishing final relative momentum.

1.6 Example: neutron capture on ^{238}U

Consider radiative capture

$$n + {}^{238}\mathrm{U} \longrightarrow {}^{239}\mathrm{U}^{*} \longrightarrow {}^{239}\mathrm{U} + \gamma. \tag{1.27}$$

Using evaluated atomic masses, the ground-state Q-value is

$$Q = \big(m_n + m({}^{238}\mathrm{U}) - m({}^{239}\mathrm{U})\big)c^2 \approx 4.806\,\mathrm{MeV} \qquad \text{(evaluated value)}. \tag{1.28}$$

In the laboratory the target is at rest. Momentum conservation requires the compound nucleus to carry the neutron's momentum p_n. The residual kinetic energy is

$$K_U = \frac{p_n^2}{2m_U} = K_n \frac{m_n}{m_U}. \tag{1.29}$$

Energy balance for forming ^{239}U at excitation ΔE reads

$$K_n + Q = K_U + \Delta E = K_n \frac{m_n}{m_U} + \Delta E, \tag{1.30}$$

so

$$\Delta E = Q + K_n\Big(1 - \frac{m_n}{m_U}\Big) \approx Q + K_n \qquad (m_n \ll m_U). \tag{1.31}$$

For a **thermal** neutron ($K_n \approx 0$),

$$\Delta E \approx Q \approx 4.806\,\mathrm{MeV}. \tag{1.32}$$

Capture therefore populates levels of ^{239}U near 4.806 MeV of excitation. Discrete levels above that energy are reached by increasing K_n. When K_n matches a compound-nucleus resonance, the capture cross section rises sharply. The energy dependence of $\sigma(K_n)$ shows a series of peaks: **neutron resonances**. Levels below S_n are not populated by capture of free neutrons, because even $K_n = 0$ already deposits $\sim Q$ [6, 1, 2, 27, 20, 21].

Remark

The same $Q \approx 4.806\,\mathrm{MeV}$ sets the neutron separation energy of ^{239}U: $S_n({}^{239}\mathrm{U}) = Q$. Resonances just above S_n dominate low-energy neutron physics of ^{238}U and enter reactor design [6, 1, 35, 33].

1.7 Cross section versus energy: resonances (concept)

Plotting σ against incident energy for a fixed channel often reveals narrow peaks. Each peak corresponds to a quasi-stationary state of the compound system whose energy matches the available CM energy. Qualitatively:

- on resonance, the reaction probability is large;
- off resonance, other processes (potential scattering, direct channels) may dominate.

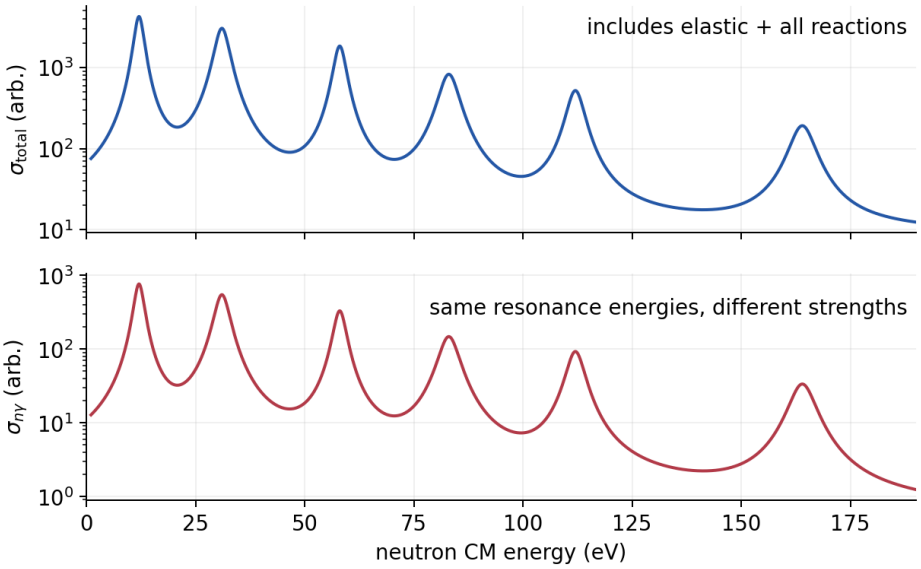

Figure 1.2: Schematic distinction between the evaluated *total* neutron cross section and the (n,γ) partial cross section for ^{238}U. Resonance energies can coincide while peak heights and backgrounds differ because the total includes elastic and every open reaction channel. Curves are redrawn for instruction and are not evaluated numerical data [35].

The line shape follows by writing a resonant amplitude with pole $E_R - i\Gamma/2$. An entrance wave in partial wave J supplies the geometrical area π/k_i^2 and spin fraction $g_J = (2J+1)/[(2j_a+1)(2j_A+1)]$. Formation contributes the entrance branching amplitude $\sqrt{\Gamma_i}$, decay contributes $\sqrt{\Gamma_f}$, and propagation contributes $(E - E_R + i\Gamma/2)^{-1}$. Squaring this product gives, for an isolated level of spin J, entrance channel $i = a + A$, and exit channel $f = b + B$, the single-level **Breit–Wigner** cross section is

$$\sigma_{i\to f}(E) = \frac{\pi}{k_i^2}\, g_J\, \frac{\Gamma_i \Gamma_f}{(E - E_R)^2 + (\Gamma/2)^2}, \qquad g_J = \frac{2J+1}{(2j_a+1)(2j_A+1)}, \tag{1.33}$$

If the integrated final-state cross section counts an unordered pair of identical particles once, multiply the right-hand side by $1/S_f$, where $S_f = 1 + \delta_{bB}$. The entrance flux has no such division; this convention must be used consistently in the inverse reaction. Here $k_i = p_i/\hbar$, E_R is the CM resonance energy, Γ_i and Γ_f are partial widths, and $\Gamma = \sum_c \Gamma_c$. At the peak, $\sigma_{i\to f}(E_R) = (4\pi/k_i^2) g_J (\Gamma_i/\Gamma)(\Gamma_f/\Gamma)$: formation and decay branching both matter. The lifetime is

$$\tau \sim \frac{\hbar}{\Gamma}: \tag{1.34}$$

narrow resonances live longer. Energy-dependent penetrabilities can make $\Gamma_c(E)$ vary across a peak, while overlapping levels and a direct amplitude produce interference beyond the isolated-resonance approximation. The kinematic message is that discrete ΔE values map to discrete K_b peaks and incident formation energies [6, 14, 2].

1.8 Inverse reactions and detailed balance

The inverse of $a + A \to b + B$ is $b + B \to a + A$, and

$$Q_{\text{inverse}} = -Q_{\text{forward}}. \tag{1.35}$$

Time-reversal invariance does *not* say that the two cross sections are numerically equal: incident flux, phase space, and spin multiplicities differ. For unpolarized massive two-body channels at the same total CM energy, define $g_i = (2j_a + 1)(2j_A + 1)$, $g_f = (2j_b + 1)(2j_B + 1)$, and $S_i = 1 + \delta_{aA}$, $S_f = 1 + \delta_{bB}$. If each identical final pair is counted once, reciprocity gives

$$g_i\, p_i^2\, S_f\, \sigma_{aA\to bB} = g_f\, p_f^2\, S_i\, \sigma_{bB\to aA}. \tag{1.36}$$

Both cross sections must correspond to the same nuclear states and invariant energy.

Photon channel. A real photon has two transverse polarization states, not $2j_\gamma + 1 = 3$. For $a + A \leftrightarrow B + \gamma$, with distinct a, A and unpolarized beams/targets, the separately averaged capture and photodisintegration cross sections obey

$$(2j_a + 1)(2j_A + 1)\, p_{aA}^2\, \sigma_{aA\to B\gamma} = 2(2J_B + 1)\, p_\gamma^2\, \sigma_{\gamma B\to aA}, \tag{1.37}$$

where $p_\gamma = E_\gamma/c$. If a photon cross section is quoted for one fixed polarization rather than averaged over both, the factor 2 must be changed accordingly; identical massive particles require the S factors of Eq. (1.36). This polarization formula, rather than a formal substitution $j_\gamma = 1$ into the massive-particle expression, is used to connect capture and photodisintegration [6, 14].

Key idea

Students should remember:

- $Q = (m_a + m_X - m_b - m_Y)c^2$; $Q + K_a = K_b + K_Y + \Delta E$.
- Eliminate K_Y with $p_Y^2 = p_a^2 + p_b^2 - 2p_a p_b \cos\theta$.
- ΔE from measured K_b, θ, K_a via (1.17).
- Endothermic threshold: $K_a^{\text{th}} \simeq (-Q + \Delta E)(1 + m_a/m_X)$; use (1.24) for the exact result.
- $n + {}^{238}\text{U}$: $Q \simeq 4.806\,\text{MeV}$ sets capture excitation for slow neutrons; resonances map levels above S_n.
- Cross section peaks at compound resonances (Breit–Wigner shape).
- Inverse reactions have opposite Q-values; detailed balance also includes spin weights and CM momenta.

1.9 Deeper physics: Q-value kinematics and reaction thresholds

1.9.1 Two-body Q and energy release

For a reaction $X(a,b)Y$, the Q-value is

$$Q = [M(X) + M(a) - M(b) - M(Y)]c^2, \tag{1.38}$$

using atomic masses when the participants are neutral atoms [6, 1]. If $Q > 0$ the reaction is exothermic: rest mass converts to kinetic energy of the products. If $Q < 0$ the reaction is endothermic and requires a minimum projectile energy (threshold) before it can occur. The two-body kinematic relations in the lecture connect Q to the measured kinetic energies of a and b in the laboratory frame [6, 14].

Threshold for $^{13}\mathrm{C}(p,\gamma)^{14}\mathrm{N}$

The ground-state capture has $Q \approx 7.55\,\mathrm{MeV}$ [6, 20]. Because the proton and target are both massive, the threshold laboratory energy E_{th} exceeds $|Q|$ when $Q < 0$; for exothermic capture, $Q > 0$ and the reaction is possible at zero projectile energy in principle. In practice, Coulomb barrier penetration requires $E_p \gtrsim 0.5\,\mathrm{MeV}$ for this channel in stellar hydrogen burning (Lecture 26) [36].

1.9.2 Threshold energy for endothermic reactions

When $Q < 0$, define $|Q|$ as the energy deficit. In the centre-of-mass frame the minimum kinetic energy that conserves momentum is

$$E_{\mathrm{th}} = |Q|\left(1 + \frac{m_a}{M_X}\right), \tag{1.39}$$

for a target at rest [6, 1]. The extra factor m_a/M_X supplies the recoil energy of the target: not all projectile energy is available to create the heavier product. For neutron-induced reactions ($m_a \ll M_X$) the threshold is nearly $|Q|$; for proton beams on heavy targets the correction can be tens of percent [14].

Key idea

From thresholds to fission and fusion. Endothermic thresholds govern which channels open as beam energy rises: the first excited state of Y adds $|Q|$ to the threshold. In fission, $Q > 0$ for actinides but a saddle barrier must still be surmounted (Lecture 23). In fusion, even exothermic reactions require tunneling through the Coulomb barrier (Lecture 25). Two-body kinematics is the common language linking all three domains [6, 2].

1.9.3 Centre-of-mass versus laboratory observables

Reaction cross sections and angular distributions are simplest in the CM frame, where momentum conservation is symmetric. Laboratory angles must be transformed when comparing data from inverse kinematics, where the heavy nucleus is the projectile [6, 1]. The Q-value is Lorentz

invariant, but the kinetic-energy partition between products is not: the same $Q > 0$ capture reaction deposits more recoil energy in the target when the projectile is light (neutron capture) than when it is heavy (inverse kinematics with a radioactive beam) [14, 51]. Evaluated masses from AME2020 fix Q to keV precision; threshold calculations should use those values rather than SEMF estimates [27, 20].

1.9.4 Recoil and the light-particle limit

When the projectile is much lighter than the target ($m_a \ll M_X$), the centre-of-mass frame is nearly at rest in the laboratory and the target recoil is negligible. Neutron-induced reactions are the standard example: the Q-value appears almost entirely as product kinetic energy [6, 35]. When the projectile is comparable to or heavier than the target (inverse kinematics), laboratory-frame observables must be transformed carefully before extracting Q or excitation energies [51, 1]. Alpha-decay recoil (Lecture 16) is the single-body limit of the same momentum bookkeeping.

Jacobian singularities near kinematic extrema amplify cross-section uncertainties when transforming between frames. In inverse kinematics, a 1 mrad angular error near zero degrees can dominate the excitation-energy budget. Document angle calibration with elastic scattering peaks before trusting missing-mass spectra.

1.10 Further physics from the literature

Relativistic two-body kinematics. At beam energies of tens to hundreds of MeV per nucleon the non-relativistic reduction $p^2 = 2mK$ fails. Exact Lorentz-invariant s-channel kinematics replace (1.17); the Källén function in (1.10) supplies the exact two-body momentum. Modern analysis codes implement the full transformation between laboratory and CM frames [6, 14].

Missing-mass spectroscopy. When only particle b is detected, the missing mass of Y is reconstructed from four-momentum conservation. Peaks in the missing-mass spectrum are excited states of Y. The method is standard at intermediate-energy facilities [6, 1]. Explicitly,

$$M_{\mathrm{miss}}^2 c^4 = (E_a + m_X c^2 - E_b)^2 - c^2 |\mathbf{p}_a - \mathbf{p}_b|^2, \qquad \Delta E = (M_{\mathrm{miss}} - m_Y)c^2.$$

This invariant form avoids assigning a non-relativistic recoil correction outside its range of validity.

R-matrix and Breit–Wigner parameters. Isolated resonances are parameterised by E_R, partial widths Γ_c, and channel radii in R-matrix theory. Overlapping resonances and direct–resonance interference require more elaborate treatments [6, 14, 2].

Reactor and astrophysical capture. The $^{238}\mathrm{U}(n,\gamma)$ resonances control neutron economy in reactors. In astrophysics, (n,γ) rates on unstable nuclei set the s- and r-process paths; many rates are still extrapolated from statistical models constrained by stable-target data [6, 1, 2, 35].

Evaluated-data cross-check. The lecture's rounded 4.86 MeV capture energy has been corrected to $S_n(^{239}\mathrm{U}) \simeq 4.806\,\mathrm{MeV}$. Evaluated masses should be used for numerical Q-values, while evaluated reaction libraries should be used for resonance parameters; a plotted total cross section is not automatically the (n,γ) partial cross section [33, 35].

Reading guide

Krane [6] Ch. 11 (kinematics, Q-values, thresholds, resonances); Dunlap [1] (worked kinematic examples); Basdevant [14] (resonances); Demtröder [2] (neutron physics); Verma [32], Nuclear Reaction Parts 1–3. Mass tables and evaluated levels: AME / NuDat [20, 21].

1.10.1 Relativistic Q-values and missing mass

When beam energies exceed tens of MeV per nucleon, the non-relativistic relation $p^2 = 2mK$ fails. The invariant mass squared of the initial state,

$$s = \left(E_a + M_X c^2\right)^2 - |\mathbf{p}_a|^2 c^2, \tag{1.40}$$

fixes the centre-of-mass energy available for reaction [6, 14]. Missing-mass spectroscopy reconstructs the excitation energy of Y when only particle b is detected:

$$M_{\mathrm{miss}}^2 c^4 = (E_a + M_X c^2 - E_b)^2 - c^2|\mathbf{p}_a - \mathbf{p}_b|^2. \tag{1.41}$$

Peaks in M_{miss} map excited states of Y without detecting the recoil [1, 6].

Threshold for $^{238}\mathrm{U}(n,f)$

Neutron-induced fission of ^{238}U has $Q \approx 6.5\,\mathrm{MeV}$ but requires $E_n \gtrsim 1\,\mathrm{MeV}$ in practice because the fission barrier $B_f \approx 6\,\mathrm{MeV}$ must be surmounted (Lecture 23) [6, 35]. The reaction threshold in (1.39) applies to endothermic channels; fission adds a saddle barrier on top of the Q-value bookkeeping. Fast-reactor spectra extend above this threshold, converting fertile ^{238}U to fissile ^{239}Pu via (n,γ) followed by β^- decay (Lecture 24) [1].

1.10.2 From kinematics to astrophysical rates

Radiative-capture Q-values set the energy of emitted γ rays and determine whether a channel is exothermic at stellar temperatures. The $^{12}\mathrm{C}(p,\gamma)^{13}\mathrm{N}$ reaction in the CNO cycle and $^3\mathrm{He}(^3\mathrm{He},2p)^4\mathrm{He}$ in the pp chain (Lecture 26) are exothermic with $Q > 0$ but still require tunneling through the Coulomb barrier (Lecture 25) [36, 6]. Inverse kinematics with radioactive beams reverses the roles of projectile and target but uses the same invariant-mass algebra [51, 52].

Key idea

Arc through the course. Two-body kinematics links α-decay recoil (Lecture 16), β endpoints (Lecture 18), direct-reaction energy sharing (Lecture 21), fission thresholds (Lectures 23–24), and Gamow-peak integrals (Lecture 26). Evaluated masses from AME2020 anchor every Q-value in the chain [27, 6].

1.10.3 Resonances and the Q scale in capture reactions

When a compound level sits near the threshold energy, the cross section is enhanced by a Breit–Wigner factor (Lecture 21) [6, 14]. The $^{238}\mathrm{U}(n,\gamma)$ resonances that control reactor neutron economy are sharp because the neutron width is small compared with level spacing [35, 6]. In astrophysics, radiative capture on unstable nuclei often relies on statistical estimates anchored by stable-target data; the Q-value from AME2020 sets the absolute energy scale for those extrapolations [27, 51]. Missing-mass spectroscopy with radioactive beams is the modern implementation of the same two-body kinematics in inverse geometry [14, 2].

1.10.4 Inverse kinematics and radioactive beams

When the heavy nucleus is the projectile, laboratory angles are compressed into a forward cone and energy loss in the target smears the excitation-energy resolution [51, 1]. Missing-mass reconstruction remains the standard tool because detecting the heavy recoil is often impractical. Active-target time-projection chambers place the reaction vertex inside an extended gas volume, so vertex reconstruction and energy-loss corrections become part of the kinematics chain [52, 6]. The ideal two-body formulas of the main lecture are therefore the first step in an analysis notebook that lists corrections explicitly rather than treating them as afterthoughts.

1.11 Deeper reading: Q values, thresholds, and missing mass

Two-body kinematics converts measured angles and momenta into excitation energy once Q is known from masses. Thresholds for populating excited states follow by adding E_x to the ground-state endothermicity. Inverse kinematics with radioactive beams boosts forward focusing and demands careful angular-resolution budgets near zero degrees.

Missing-mass reconstruction uses the undetected recoil's inferred four-momentum; invariant-mass methods use decay products of unbound states. Active-target TPCs add vertex and energy-loss corrections on top of the ideal two-body map. Always compute Q from AME masses before simulating a spectrometer acceptance.

Inclusive versus exclusive

Inclusive measurements integrate over unobserved particles and need careful efficiency modelling; exclusive two-body measurements lean on this chapter's algebra. Missing-mass resolution is limited by beam energy spread, target thickness, and angle. Quote the resolution budget when claiming a new excited state.

Threshold cusps

Opening a new channel redistributes flux and can produce cusps or rounded steps in excitation functions. Interpreting those features requires the Q-value map of Lecture 22 together with continuum coupling ideas from Lectures 10 and 21.

Kinematic lab exercise

Pick $^{12}\mathrm{C}(p,p')^{12}\mathrm{C}^*$ to the first 2^+ state. Compute Q for elastic and inelastic channels, the threshold beam energy, and the laboratory scattering angle corresponding to a given centre-of-mass angle at one beam energy. Propagate a 0.1° angle error into E_x near the kinematic limit.

Repeat in inverse kinematics for a hypothetical radioactive beam on a proton target. Observe the forward focusing and the heightened angle sensitivity. This pair of calculations is the everyday toolkit for spectrometer design and for understanding why missing-mass resolution budgets are dominated by angles and energy loss rather than by algebra errors in Q.

Kinematics is the map between detector coordinates and nuclear excitation. Inverse kinematics and missing mass are applications of the same two-body algebra.

In practice, rework one numerical estimate from the lecture with a different parameter set and compare the shift to the quoted experimental uncertainty. If the shift exceeds the uncertainty, the estimate is teaching a scale, not delivering a fit. That distinction keeps theoretical cartoons honest when they sit beside evaluated data tables and modern many-body calculations. Along the course arc, write one sentence linking this chapter backward and one forward: the discipline of those two sentences is as important as any single formula. Examination problems rarely ask for a literature review, but they do ask for the scale argument that literature reviews presuppose.

Synthesis problem

Write a half-page note that (i) restates the chapter's central scale or selection rule in one equation, (ii) evaluates it numerically for one concrete nucleus or energy, and (iii) names the neighbouring lecture that uses the result. Keep the note free of research-frontier speculation; the goal is fluency with the lecture physics itself. If an assumption fails (Born approximation, spherical mean field, allowed transition, one-dimensional barrier), state the failure mode in a final sentence. That habit converts passive reading into examination-ready understanding and makes the later research-frontier box read as an extension rather than a replacement.

Research frontier: inverse kinematics and missing-mass methods

Two-body kinematics (Lecture 22) is indispensable for inverse-kinematics experiments with radioactive beams, active-target time-projection chambers, and storage-ring reactions. Missing-mass spectroscopy reconstructs excitation energies when the recoil is undetected; thresholds and Q values from AME2020 set the absolute energy scale [27, 51]. Facility upgrades emphasise high-rigidity spectrometers and storage rings precisely because kinematic acceptance and luminosity limit the reach to the most exotic beams [52]. Uncertainties that students should watch for in published analyses include angular-resolution propagation near zero degrees, target thickness and energy-loss corrections, and the difference between missing-mass and invariant-mass reconstructions for unbound states. The lecture's two-body algebra is therefore not merely homework: it is the everyday language of radioactive-beam proposals and spectrometer design.

Active-target TPCs blur the lecture's sharp "thin-target" idealisation because the reaction vertex sits inside an extended gas volume. Reconstructing the vertex and correcting energy loss become part of the kinematics chain. Understanding two-body relations first makes those corrections intelligible rather than mysterious.
Vertex reconstruction and energy-loss corrections turn the ideal two-body formulas into the real analysis chain of an active-target experiment.
Writing the ideal kinematic map first, then listing corrections, is the recommended analysis notebook structure.
Spectrometer design documents for FRIB and FAIR make the same kinematic trade-offs explicit when choosing angular coverage and rigidity.
Student directions. (1) Kinematics exercise: for a given $X(a,b)Y$ reaction, compute Q and the threshold for the first excited state of Y. (2) Error propagation: show how a 1 mrad angular error propagates into K_b near zero degrees in inverse kinematics. (3) Methods comparison: contrast missing-mass and invariant-mass methods for unbound resonant states.

1.12 Problems with solutions

Problem 22.1: Q-value from masses

Using rest energies $m_a c^2 = 938.3\,\text{MeV}$, $m_X c^2 = 11174.9\,\text{MeV}$, $m_b c^2 = 1875.6\,\text{MeV}$, $m_Y c^2 = 10252.5\,\text{MeV}$, compute Q for $a + X \to b + Y$. Is the reaction exoergic or endoergic? [6]

Solution 22.1

$$Q = (938.3 + 11174.9) - (1875.6 + 10252.5) = 12113.2 - 12128.1 = -14.9\,\text{MeV}.$$

Endoergic ($Q < 0$).

Problem 22.2: Threshold energy

For a reaction with $Q = -14.9\,\text{MeV}$, $\Delta E = 0$, projectile mass number $A_a = 1$, target $A_X = 12$, find the laboratory threshold K_a^{th} [6, 1].

Solution 22.2

$$K_a^{\text{th}} = (-Q)\Big(1 + \frac{m_a}{m_X}\Big) = 14.9\Big(1 + \frac{1}{12}\Big) = 14.9 \times \frac{13}{12} = 16.1\,\text{MeV}.$$

Problem 22.3: Residual momentum

In a reaction at $\theta = 30^\circ$, $p_a = 150\,\text{MeV}/c$, $p_b = 120\,\text{MeV}/c$. Find p_Y from momentum conservation [1].

Solution 22.3

$$p_Y^2 = p_a^2 + p_b^2 - 2p_a p_b \cos\theta = 150^2 + 120^2 - 2(150)(120)\cos 30^\circ.$$

$$\cos 30^\circ = \sqrt{3}/2 \approx 0.866, \qquad 2(150)(120)(0.866) = 31176.$$

$$p_Y^2 = 22500 + 14400 - 31176 = 5724, \qquad p_Y = 75.7\,\text{MeV}/c.$$

Problem 22.4: Excitation from K_b (forward angle)

For $n + {}^{12}\text{C} \to n' + {}^{12}\text{C}^*$ treat the inelastic neutron as $a = b = n$, $X = Y = {}^{12}\text{C}$, $Q = 0$. At $\theta = 0$ and $K_a = 20.0\,\text{MeV}$, a peak is found at $K_b = 15.5\,\text{MeV}$. Estimate ΔE using $\Delta E \approx K_a - K_b$ (heavy residual, forward kinematics), then correct with the leading recoil terms of (1.17) using $m_n/m_C = 1/12$ [6].

Solution 22.4

Crude estimate:

$$\Delta E \approx 20.0 - 15.5 = 4.5\,\text{MeV}.$$

With $Q = 0$, $m_a = m_b = m_n$, $m_Y = m_C$, $\theta = 0$, $\cos\theta = 1$,

$$\Delta E = -K_b\Big(1 + \frac{1}{12}\Big) + K_a\Big(1 - \frac{1}{12}\Big) + \frac{2}{12}\sqrt{K_a K_b}$$
$$= -15.5 \times \frac{13}{12} + 20.0 \times \frac{11}{12} + \frac{1}{6}\sqrt{20 \times 15.5}.$$

$$\sqrt{310} \approx 17.61, \quad \frac{1}{6} \times 17.61 \approx 2.94,$$

$$\Delta E = -16.79 + 18.33 + 2.94 = 4.48\,\text{MeV}.$$

The residual is excited by about 4.5 MeV.

Problem 22.5: Thermal capture on ^{238}U

Show that a neutron with $K_n = 0.025\,\text{eV}$ on ^{238}U produces essentially the same excitation as a zero-energy neutron if $Q = 4.806\,\text{MeV}$. Compute ΔE from (1.31) [6, 1].

Solution 22.5

$$\frac{m_n}{m_U} \approx \frac{1}{239} \approx 4.2 \times 10^{-3}, \qquad K_n = 2.5 \times 10^{-8}\,\text{MeV}.$$

$$\Delta E = Q + K_n\Big(1 - \frac{m_n}{m_U}\Big) = 4.806\,\text{MeV} + 2.5 \times 10^{-8}\,\text{MeV} \times 0.996 \approx 4.806\,\text{MeV}.$$

Thermal kinetic energy is negligible next to Q.

Problem 22.6: Resonance and lifetime

A neutron resonance has total width $\Gamma = 0.10\,\text{eV}$. Estimate the compound-state lifetime $\tau = \hbar/\Gamma$. Use $\hbar = 6.58 \times 10^{-16}\,\text{eV}\cdot\text{s}$ [6, 14].

Solution 22.6

$$\tau = \frac{6.58 \times 10^{-16}\,\text{eV}\cdot\text{s}}{0.10\,\text{eV}} = 6.6 \times 10^{-15}\,\text{s}.$$

This is a long-lived compound resonance, far longer than a direct transit time $\sim 10^{-22}\,\text{s}$. Compound lifetimes span a broad range because the widths of individual levels span a broad range.

Problem 22.7: Why excited residuals lower K_b

From $Q + K_a = K_b + K_Y + \Delta E$, explain why peaks corresponding to higher ΔE appear at lower K_b in a fixed-angle spectrum for fixed K_a [6, 1].

Solution 22.7

For fixed entrance energy K_a and fixed Q, the sum $K_b + K_Y + \Delta E$ is fixed. Increasing ΔE reduces the kinetic energy available to share between b and Y. At a fixed angle the kinematic solution for K_b therefore decreases: excited-state peaks sit at lower detected energy than the ground-state peak. That is the basis of missing-mass / reaction spectroscopy.

Problem 22.8: Exact versus non-relativistic threshold

For $a + X \to b + Y$, take $Q = -20.0\,\text{MeV}$, $m_a c^2 = 938.3\,\text{MeV}$, $m_X c^2 = 11174.9\,\text{MeV}$, and $\Delta E = 2.0\,\text{MeV}$. Find (a) the non-relativistic threshold, (b) the exact correction, and (c) their fractional difference [6, 14].

Solution 22.8

Step 1: effective Q-value.

$$Q^* = Q - \Delta E = -22.0\,\text{MeV}.$$

Step 2: leading threshold.

$$K_{\text{th}}^{\text{NR}} = -Q^*\left(1 + \frac{m_a}{m_X}\right) = 22.0\left(1 + \frac{938.3}{11174.9}\right) = 23.85\,\text{MeV}.$$

Step 3: exact mass correction.

$$\delta K_{\text{rel}} = \frac{(Q^*)^2}{2m_X c^2} = \frac{(22.0)^2}{2(11174.9)} = 0.0217\,\text{MeV}.$$

Hence

$$K_{\text{th}}^{\text{exact}} = 23.87\,\text{MeV}, \qquad \frac{\delta K_{\text{rel}}}{K_{\text{th}}^{\text{NR}}} = 9.1 \times 10^{-4}.$$

The correction is small here, but the invariant derivation identifies it and remains valid when the non-relativistic approximation does not.

Problem 22.9: Reciprocity of an inverse reaction

At one CM energy, suppose a and A have spins $1/2$ and 0, while b and B have spins 0 and 1. If $p_i = 60\,\text{MeV}/c$, $p_f = 90\,\text{MeV}/c$, and $\sigma_{aA\to bB} = 12\,\text{mb}$, find $\sigma_{bB\to aA}$. Assume no identical-particle factors [6].

Solution 22.9

Step 1: spin statistical weights.

$$g_i = (2\tfrac{1}{2}+1)(2\cdot 0+1) = 2, \qquad g_f = (2\cdot 0+1)(2\cdot 1+1) = 3.$$

Step 2: apply detailed balance.

$$g_i p_i^2 \sigma_{i\to f} = g_f p_f^2 \sigma_{f\to i},$$

so

$$\sigma_{f\to i} = \frac{g_i}{g_f}\frac{p_i^2}{p_f^2}\sigma_{i\to f} = \frac{2}{3}\left(\frac{60}{90}\right)^2 (12\,\text{mb}) = 3.56\,\text{mb}.$$

The inverse cross section is smaller even though the transition matrix element is constrained by time reversal, because flux, phase space, and spin multiplicities differ.

Problem 22.10: Breit–Wigner peak and area

An isolated resonance has $g_J = 1$, $k = 0.50\,\text{fm}^{-1}$, $\Gamma_i = 0.20\,\text{eV}$, $\Gamma_f = 0.30\,\text{eV}$, and $\Gamma = 0.80\,\text{eV}$. Find (a) the peak cross section and (b) $\int \sigma(E)\,\mathrm{d}E$, treating k and widths as constant across the line [6, 14].

Solution 22.10

$$\sigma(E_R) = \frac{4\pi}{k^2}\frac{\Gamma_i}{\Gamma}\frac{\Gamma_f}{\Gamma} = \frac{4\pi}{0.25}(0.25)(0.375) = 4.71\,\text{fm}^2 = 47.1\,\text{mb}.$$

Using $\int_{-\infty}^{\infty} \mathrm{d}x/(x^2+a^2) = \pi/a$,

$$\int \sigma(E)\,\mathrm{d}E = \frac{2\pi^2}{k^2}\frac{\Gamma_i\Gamma_f}{\Gamma} = 5.92\,\text{fm}^2\,\text{eV} = 59.2\,\text{mb}\,\text{eV}.$$

Peak height depends on branching ratios, while the resonance area also carries the absolute width scale.

Problem 22.11: Capture–photodisintegration balance

For $a(1/2) + A(0) \leftrightarrow B(1/2) + \gamma$, let $p_{aA} = 20\,\mathrm{MeV}/c$, $p_\gamma = 5\,\mathrm{MeV}/c$, and $\sigma_{aA\to B\gamma} = 10\,\mu\mathrm{b}$. Find the unpolarized inverse cross section, assuming distinct massive particles [6, 14].

Solution 22.11

The massive entrance degeneracy is $(2j_a+1)(2j_A+1) = 2$. The photon–nucleus channel has $2(2J_B+1) = 4$, where 2 counts transverse photon polarizations. Hence

$$\sigma_{\gamma B\to aA} = \frac{2(20)^2}{4(5)^2}(10\,\mu\mathrm{b}) = 80\,\mu\mathrm{b}.$$

Using $2j_\gamma + 1 = 3$ would be incorrect for a real photon.

Bibliography

[1] R. A. Dunlap, *An Introduction to the Physics of Nuclei and Particles* (2nd ed.), IOP Publishing, Bristol (2023), DOI: 10.1088/978-0-7503-6094-4, Ch. 3 (Nuclear composition and size).

[2] W. Demtröder, *Nuclear and Particle Physics*, Undergraduate Lecture Notes in Physics, Springer, Cham (2023).

[3] S. Petrera, *Problems and Solutions in Nuclear and Particle Physics*, UNITEXT for Physics, Springer, Cham (2019).

[4] F. Terranova, *A Modern Primer in Particle and Nuclear Physics*, Oxford University Press (2021).

[5] S. D'Auria, *Introduction to Nuclear and Particle Physics*, Undergraduate Lecture Notes in Physics, Springer, Cham (2018).

[6] K. S. Krane, *Introductory Nuclear Physics*, Wiley, New York (1988).

[7] R. Hofstadter, "Electron scattering and nuclear structure," Rev. Mod. Phys. **28**, 214 (1956).

[8] H. F. Ehrenberg, R. Hofstadter, U. Meyer-Berkhout, D. G. Ravenhall, and S. E. Sobottka, "High-Energy Electron Scattering and the Charge Distribution of Carbon-12 and Oxygen-16," Phys. Rev. **113**, 666 (1959).

[9] H. Yukawa, "On the interaction of elementary particles. I," Proc. Phys.-Math. Soc. Japan **17**, 48 (1935).

[10] R. D. Woods and D. S. Saxon, "Diffuse surface optical model for nucleon-nuclei scattering," Phys. Rev. **95**, 577 (1954).

[11] H. G. J. Moseley, "The high-frequency spectra of the elements," Phil. Mag. **26**, 1024 (1913); **27**, 703 (1914).

[12] C. F. von Weizsäcker, "Zur Theorie der Kernmassen," Z. Phys. **96**, 431 (1935).

[13] P. Cappellaro, *Introduction to Applied Nuclear Physics* (MIT OpenCourseWare / LibreTexts), CC BY-NC-SA 4.0.

[14] J.-L. Basdevant, J. Rich, and M. Spiro, *Fundamentals in Nuclear Physics: From Nuclear Structure to Cosmology*, Springer, New York (2005).

[15] D. Tong, *Particle Physics*, Lecture notes (University of Cambridge / CERN school notes).

[16] M. G. Mayer, "On closed shells in nuclei. II," Phys. Rev. **75**, 1969 (1949).

[17] O. Haxel, J. H. D. Jensen, and H. E. Suess, "On the "magic numbers" in nuclear structure," Phys. Rev. **75**, 1766 (1949).

[18] T. Schmidt, "Über die magnetischen Momente der Atomkerne," Z. Phys. **106**, 358 (1937).

[19] L. W. Nordheim, "On spins, moments, and shells in nuclei," Phys. Rev. **78**, 294 (1950).

[20] Evaluated Nuclear Structure Data File (ENSDF), National Nuclear Data Center, Brookhaven National Laboratory, `https://www.nndc.bnl.gov/ensdf/`.

[21] NuDat 3, National Nuclear Data Center, Brookhaven National Laboratory, `https://www.nndc.bnl.gov/nudat3/`.

[22] N. J. Stone, "Table of nuclear magnetic dipole and electric quadrupole moments," At. Data Nucl. Data Tables **90**, 75 (2005); updated compilations at NNDC.

[23] W. N. Cottingham and D. A. Greenwood, *An Introduction to Nuclear Physics* (2nd ed.), Cambridge University Press, Cambridge (2001).

[24] H. Geiger and J. M. Nuttall, "The ranges of the α particles from the radioactive substances," Phil. Mag. **22**, 613 (1911).

[25] G. Gamow, "Zur Quantentheorie des Atomkernes," Z. Phys. **51**, 204 (1928).

[26] R. W. Gurney and E. U. Condon, "Wave mechanics and radioactive disintegration," Nature **122**, 439 (1928); Phys. Rev. **33**, 127 (1929).

[27] M. Wang, W. J. Huang, F. G. Kondev, G. Audi, and S. Naimi, "The AME 2020 atomic mass evaluation (II). Tables, graphs and references," Chin. Phys. C **45**, 030003 (2021).

[28] Laboratoire National Henri Becquerel (LNHB), Recommended decay data, `http://www.lnhb.fr/nuclear-data/nuclear-data-table/`.

[29] L. M. Langer, R. D. Moffat, and H. C. Price, Jr., "Low energy beta-ray spectra: P^{32} and Cu^{64}," Phys. Rev. **76**, 1725 (1949).

[30] L. M. Langer and H. C. Price, Jr., "Shapes of the beta-spectra of the forbidden transitions of Sb^{124}, Rb^{86}, Sr^{89}, Y^{91}, and Cs^{137}," Phys. Rev. **75**, 1769 (1949).

[31] D. C. Camp and L. M. Langer, "The shape of the ^{66}Ga positron spectrum and the contribution from $0^+ \to 0^+$ transitions," Phys. Rev. **129**, 1782 (1963).

[32] H. C. Verma, *Nuclear Physics: Fundamentals and Applications*, NPTEL/IIT Kanpur lecture series, `https://hcverma.in/ncl_phy_lectures`.

[33] International Atomic Energy Agency, *LiveChart of Nuclides*, evaluated structure, decay, reaction, and fission-yield data, `https://www-nds.iaea.org/relnsd/vcharthtml/VChartHTML.html`.

[34] T. Kibédi, T. W. Burrows, M. B. Trzhaskovskaya, P. M. Davidson, and C. W. Nestor, Jr., "Evaluation of theoretical conversion coefficients using BrIcc," Nucl. Instrum. Methods Phys. Res. A **589**, 202 (2008), DOI: 10.1016/j.nima.2008.02.051.

[35] D. A. Brown *et al.*, "ENDF/B-VIII.0: The 8th major release of the nuclear reaction data library with CIELO-project cross sections, new standards and thermal scattering data," Nucl. Data Sheets **148**, 1 (2018), DOI: 10.1016/j.nds.2018.02.001.

[36] B. Acharya *et al.*, "Solar fusion III: New data and theory for hydrogen-burning stars," Rev. Mod. Phys. **97**, 035002 (2025), DOI: 10.1103/8lm7-gs18.

[37] S. N. Ghoshal, "An experimental verification of the theory of compound nucleus," Phys. Rev. **80**, 939 (1950), DOI: 10.1103/PhysRev.80.939.

[38] D. Adhikari *et al.* (PREX Collaboration), "Accurate determination of the neutron skin thickness of ^{208}Pb through parity-violation in electron scattering," Phys. Rev. Lett. **126**, 172502 (2021), DOI: 10.1103/PhysRevLett.126.172502.

[39] B. T. Reed, F. J. Fattoyev, C. J. Horowitz, and J. Piekarewicz, "Implications of PREX-II on the equation of state of neutron-rich matter," Phys. Rev. Lett. **126**, 172503 (2021), DOI: 10.1103/PhysRevLett.126.172503.

[40] B. Hu *et al.*, "Ab initio predictions link the neutron skin of ^{208}Pb to nuclear forces," Nature Phys. **18**, 1196 (2022), DOI: 10.1038/s41567-022-01715-8.

[41] E. Epelbaum, H.-W. Hammer, and U.-G. Meißner, "Modern theory of nuclear forces," Rev. Mod. Phys. **81**, 1773 (2009), DOI: 10.1103/RevModPhys.81.1773.

[42] H.-W. Hammer, S. König, and U. van Kolck, "Nuclear effective field theory: Status and perspectives," Rev. Mod. Phys. **92**, 025004 (2020), DOI: 10.1103/RevModPhys.92.025004.

[43] T. Otsuka, A. Gade, O. Sorlin, T. Suzuki, and Y. Utsuno, "Evolution of shell structure in exotic nuclei," Rev. Mod. Phys. **92**, 015002 (2020), DOI: 10.1103/RevModPhys.92.015002.

[44] H. Hergert, S. K. Bogner, T. D. Morris, A. Schwenk, and K. Tsukiyama, "The in-medium similarity renormalization group: A novel ab initio method for nuclei," Phys. Rep. **621**, 165 (2016), DOI: 10.1016/j.physrep.2015.12.007.

[45] J. M. Lattimer and M. Prakash, "The equation of state of hot, dense matter and neutron stars," Phys. Rep. **621**, 127 (2016), DOI: 10.1016/j.physrep.2015.12.005.

[46] J. M. Lattimer, "Neutron stars and the nuclear matter equation of state," Annu. Rev. Nucl. Part. Sci. **71**, 433 (2021), DOI: 10.1146/annurev-nucl-102419-124827.

[47] B. P. Abbott *et al.* (LIGO Scientific Collaboration and Virgo Collaboration), "GW170817: Observation of gravitational waves from a binary neutron star inspiral," Phys. Rev. Lett. **119**, 161101 (2017), DOI: 10.1103/PhysRevLett.119.161101.

[48] M. J. Dolinski, A. W. P. Poon, and W. Rodejohann, "Neutrinoless double-beta decay: Status and prospects," Annu. Rev. Nucl. Part. Sci. **69**, 219 (2019), DOI: 10.1146/annurev-nucl-101918-023407.

[49] M. Agostini, G. Benato, J. A. Detwiler, J. Menéndez, and F. Vissani, "Toward the discovery of matter creation with neutrinoless $\beta\beta$ decay," Rev. Mod. Phys. **95**, 025002 (2023), DOI: 10.1103/RevModPhys.95.025002.

[50] P. Gysbers *et al.*, "Discrepancy between experimental and theoretical β-decay rates resolved from first principles," Nature Phys. **15**, 428 (2019), DOI: 10.1038/s41567-019-0450-7.

[51] H. L. Crawford, K. Fossez, S. König, and A. Spyrou, "A vision for the science of rare isotopes," Annu. Rev. Nucl. Part. Sci. **74**, 141 (2024), DOI: 10.1146/annurev-nucl-121423-091501.

[52] Nuclear Science Advisory Committee, *A New Era of Discovery: The 2023 Long Range Plan for Nuclear Science*, U.S. Department of Energy and National Science Foundation (2023), `https://nuclearsciencefuture.org/`.

[53] S. A. Giuliani, Z. Matheson, W. Nazarewicz, E. Olsen, P.-G. Reinhard, J. Sadhukhan, B. Schuetrumpf, N. Schunck, and P. Schwerdtfeger, "Colloquium: Superheavy elements: Oganesson and beyond," Rev. Mod. Phys. **91**, 011001 (2019), DOI: 10.1103/RevModPhys.91.011001.

[54] N. Schunck and D. Regnier, "Theory of nuclear fission," Prog. Part. Nucl. Phys. **125**, 103963 (2022), DOI: 10.1016/j.ppnp.2022.103963.

[55] I. Counts, J. Hur, D. P. L. Aude Craik, H. Jeon, C. Leung, J. C. Berengut, A. Geddes, A. Kawasaki, W. Jhe, and V. Vuletić, "Evidence for nonlinear isotope shift in Yb^+ search for new boson," Phys. Rev. Lett. **125**, 123002 (2020), DOI: 10.1103/PhysRevLett.125.123002.

[56] I. Angeli and K. P. Marinova, "Table of experimental nuclear ground state charge radii: An update," At. Data Nucl. Data Tables **99**, 69 (2013), DOI: 10.1016/j.adt.2011.12.006.

[57] S. Kraemer *et al.*, "Observation of the radiative decay of the ^{229}Th nuclear clock isomer," Nature **617**, 706 (2023), DOI: 10.1038/s41586-023-05894-z.